

Research Article

ECG Multilead QT Interval Estimation Using Support Vector Machines

Jhosmary Cuadros¹, Nelson Dugarte,² Sara Wong,³ Pablo Vanegas,³ Villie Morocho¹,³ and Rubén Medina¹²

¹Department of Electronics Engineering, Universidad Técnica Federico Santa María, Valparaíso, Chile

²Research Center for Biomedical Engineering and Telemedicine, Electrical Engineering Department, Universidad de Los Andes, Mérida, Venezuela

³Computer Science Department, Engineering School, Universidad de Cuenca, Cuenca, Ecuador

Correspondence should be addressed to Jhosmary Cuadros; jhosmary.cuadros@sansano.usm.cl

Received 31 October 2018; Revised 27 January 2019; Accepted 12 February 2019; Published 15 April 2019

Academic Editor: Jose Joaquin Rieta

Copyright © 2019 Jhosmary Cuadros et al. This is an open access article distributed under the Creative Commons Attribution License, which permits unrestricted use, distribution, and reproduction in any medium, provided the original work is properly cited.

This work reports a multilead QT interval measurement algorithm for a high-resolution digital electrocardiograph. The software enables off-line ECG processing including QRS detection as well as an accurate multilead QT interval detection algorithm using support vector machines (SVMs). Two fiducial points (Q_{ini} and T_{end}) are estimated using the SVM algorithm on each incoming beat. This enables segmentation of the current beat for obtaining the P, QRS, and T waves. The QT interval is estimated by updating the QT interval on each lead, considering shifting techniques with respect to a valid beat template. The validation of the QT interval measurement algorithm is attained using the Physionet PTB diagnostic ECG database showing a percent error of 2.60 ± 2.25 msec with respect to the database annotations. The usefulness of this software tool is also tested by considering the analysis of the ECG signals for a group of 60 patients acquired using our digital electrocardiograph. In this case, the validation is performed by comparing the estimated QT interval with respect to the estimation obtained using the Cardiosoft software providing a percent error of 2.49 ± 1.99 msec.

1. Introduction

Cardiovascular diseases are the leading cause of death globally, and they are also the first motivation for medical consultation. This health problem increases the need for medical service and has an important impact on health costs [1]. Among the different cardiovascular diseases, the arterial hypertension (HTA) [2], the coronary artery disease (CAD) [3], and the ischemic cardiomyopathy [4] are the most common. In particular, Chagas heart disease [5] is a parasite disease caused by the protozoan *Trypanosoma cruzi* leading to a progressive cardiac damage such as cardiomyopathy [6]. The disease is characterized by heart failure disease, arrhythmias that may predispose to systemic thromboembolism or sudden death, and atrioventricular block. The most frequent electrocardiographic abnormalities in patients with Chagas disease are ventricular extrasystole,

complete block of right branch of His bundle, atrioventricular block, and ventricular fibrillation [7]. Chagas disease is also related to other cardiovascular diseases such as arterial hypertension and coronary artery disease [8]. However, the abnormalities vary depending on geographical region and status of the disease in each patient. The distribution of Chagas has changed in recent years due to permanent migrations [9].

In Chagas disease, one of the alterations that affect the electrocardiogram (ECG) signal is the abnormal variation of intervals such as the QT interval and morphology of the T wave expressed by their residuum [10]. The QT interval represents the ventricular depolarization and repolarization time interval. This interval is measured from the Q onset to the T end. As the QT interval decreases while the heart rate increases, the QT interval is usually normalized with respect to the heart rate, and it is denoted as QTc. The accuracy in the

estimation of the *QT* interval depends on the accuracy in identification of *Q* onset and *T* end [11]. Accurate measurement of the *QT* interval could be difficult for some *T*-wave morphologies and noisy electrocardiogram signals [12]. Several research groups have shown that advanced high-resolution ECG (HRECG) processing enables the estimation of several advanced indexes related to cardiovascular diseases. The study of HRECG started in the seventies with the goal of noninvasive detection of electrical activity of the His-Purkinje system [13]. Later, other cardiac zones or ECG intervals included micropotentials related with pathological conduction of the heart [14].

Starc and Schlegel [15] have developed a system that enables real-time assessment of the *QT* interval variability in the eight independent leads of a standard electrocardiogram. This system includes hardware that performs the ECG signal acquisition at 1000 samples per second in each lead with a resolution of 12 bits per sample. The system also includes advanced HRECG software for estimating the score of reduced amplitude zones (RAZ) as well as heart rate variability (HRV) analysis either in time domain or in frequency domain. Among the advanced tools for ECG analysis, it includes the *T*-wave morphological multilead analysis based on principal component analysis (PCA). Based on this system, Schlegel et al. [16] have derived an advanced ECG score for prediction of coronary artery disease (CAD) which is based on a set of parameters estimated using the advanced software analysis. The software system known as Cardiosoft [17] runs on the windows operating system.

Karjalainen et al. [18] developed a method for quantifying the *QT* interval variability. The method is based on a technique known as principal component regression (PCR). This method allows reducing the dimensionality of data. The variation of the *QT* interval is proportional to the variation in a parameter representing the third eigenvalue of the correlation matrix. The algorithm divides the ECG signal into segments including the QRS and the *T* wave, and then, the PCR algorithm is applied. This algorithm allows studying the *QT* interval variability without detecting the *T* wave.

Christov and Simova [19] proposed an automated method that scored as second in the Physionet/CinC Challenge 2006. The method is based on analyzing the presence of peaks or slopes in two consecutive segments of 10 msec. The search is performed first for estimating the *Q* onset and then for the *T* end. A revision of several classical methods for *QT* detection is presented by Xue and Reddy [20].

The analysis of the ECG signal is becoming an important tool for the assessment of several cardiac diseases. In this context, we are proposing a system including hardware and software for HRECG analysis, where support vector machine (SVM) techniques [21–23] are used within the framework for *QT* interval estimation. The proposed system includes the signal acquisition electronics hardware as well as a software system for ECG signal analysis. The software system is based on open-source libraries and runs on the Linux operating system. The proposed system performs multilead *QT* interval estimation. The proposed methodology is based on the work reported by Starc and

Schlegel [15] but we have used a different approach for preprocessing and for segmentation of the QRS template on the eight independent leads of the 12-lead standard surface electrocardiogram. In our algorithm, rather than relying on the QRS detector for determining the beginning of the QRS (Q_{onset}) and a biparabolic curve modeling for determination at the end of the *T* wave (T_{end}), we perform these tasks using SVM techniques. The SVM learning technique is a very useful tool for classifying ECG patterns [24]. This has motivated their application for accurate estimation of this interval. The *QT* interval estimation method is validated using the Physionet PTB diagnostic ECG database [25–27], as well as a dataset including a group of 60 patients acquired using our digital electrocardiograph system. The article is organized as follows: first, a brief introduction and state of the art is given, as well as a description of the theoretical bases, and then, the methodological framework is described. Subsequently, the results are presented, and finally, conclusions are given.

2. Methods

2.1. DIGICARDIAC ECG Acquisition System. The DIGICARDIAC system enables acquisition, processing, and handling of the electrocardiogram as well as the clinical patient information. The proposed system incorporates advanced algorithms for signal processing and interval estimation as well as telemedicine tools for handling the patient electronic record. The DIGICARDIAC instrument has two types of operation modes. First of all, it can be used as any electrocardiograph in a clinical consultation. Secondly, it works as an instrument of detailed analysis, normally used in cardiac clinical research.

The electronic hardware of the DIGICARDIAC system [28] is used for acquiring the standard 12-lead electrocardiogram. This hardware system was designed to work as a whole, connected with a personal computer, as shown in Figure 1. The hardware starts working when it gets plugged into the USB port. The high-resolution electrocardiogram signals are transmitted constantly to the computer. The developed software tools running on the personal computer allow the user to initiate the electrocardiogram data recording; otherwise, the transmitted information from the hardware is discarded. The acquisition is performed using the standard 12-lead system at 2000 samples per second with a resolution of 12 bits per sample. An example of acquisition is shown in Figure 2, where the V4 recorded lead is shown.

2.1.1. Acquisition Data. The protocol included three groups of subjects: 20 patients with Chagas disease, 20 patients with hypertension, and 20 healthy subjects. Patients underwent a high-resolution 12-lead electrocardiogram (ECG) recording using DIGICARDIAC. A standard supine 12-lead ECG was recorded for 5 minutes in each of the 60 patients during normal breathing.

2.2. Multilead QT Interval Measurement. The algorithm reported for estimation of the *QT* interval is multilead in the sense that the eight independent leads of the standard

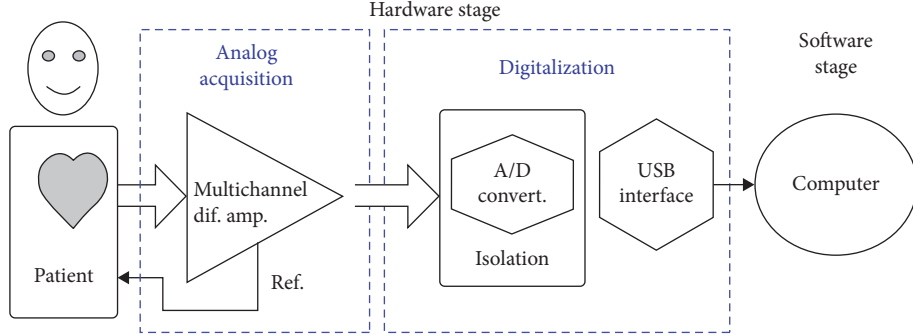


FIGURE 1: DIGICARDIAC system components.



FIGURE 2: The DIGICARDIAC user interface window showing a graphical representation of the V4 ECG lead.

electrocardiogram are considered for estimating the *QT* interval. Particularly, the segmentation of the *QRS* template as well as the incoming beat involves stages where parameters are extracted from estimations performed on each of the leads. Additionally, even when an estimation of the *QT* interval is provided as a result for each of the leads, their combination allows one to provide a representative *QT* interval estimation for all leads. A description of the different processing stages is presented in the following paragraphs.

2.2.1. Signal Preprocessing. The signal is preprocessed with a moving averaging filter for attenuating the power line interference. The baseline wandering was attenuated using a high-pass recursive filter and a FIR filter for attenuating the electromyographic noise, as reported in [19]. The phase characteristic is constant, and the filter was applied forward and then backwards for minimizing the phase distortion. The high-pass filter response is given by

$$y(n) = C_1(x(n) - x(n-1)) + C_2y(n-1), \quad (1)$$

where $x(n)$ is the input signal sequence and $y(n)$ is the output filtered sequence, and coefficients C_1 and C_2 are calculated as follows:

$$C_1 = \frac{1}{1 + \tan(f_c \pi T)}, \quad (2)$$

$$C_2 = \frac{1 - \tan(f_c \pi T)}{1 + \tan(f_c \pi T)},$$

where f_c is a cutoff frequency of 0.64 Hz and T is sampling period. The next step is using the Savitzky and Golay filter [29] for attenuating the electromyographic noise. The filter is based on performing a least-square approximation of the signal given by

$$Y(n) = \frac{1}{M} \sum_{j=-N}^N C_j X(n+j), \quad (3)$$

where $Y(n)$ and $X(n)$ are the signal after and before the least-square approximation, respectively, N is the length of the approximation interval at both sides of the sample, and C_j are the weighting approximation coefficients given by

$$C_j = 3N^2 + 3N - 1 - 5j^2, \quad (4)$$

and the normalization coefficient M is given by

$$M = \frac{(2N+1)(4n^2 + 4N - 3)}{3}. \quad (5)$$

The procedure is applied for a total interval $(2N+1)$ of 31 milliseconds. The next step during the preprocessing is the *QRS* detection, which is performed according to an adaptation of the Pan and Tompkins algorithm proposed by Mneimneh et al. [30], which uses a methodology based on thresholding. Then, a segmentation of the signal is made; this task consists in taking samples present in the ECG signal where the *QRS* complexes are present. Thus, the ECG record is divided into their component waves (a heartbeat is the representation of a cardiac cycle). The segmented ECG signals are used for constructing the *QRS* templates.

2.2.2. Templates. A histogram for the *RR* interval is constructed based on the first twenty beats extracted from the ECG signal. Then, an average *QRS* signal is obtained considering the ten beats with *RR* intervals closest to the maximum of the histogram. This averaged signal is a *QRS* template. The procedure is repeated for each of the eight independent leads of the standard electrocardiogram [15]. In Figure 3, the template for each independent lead is shown.

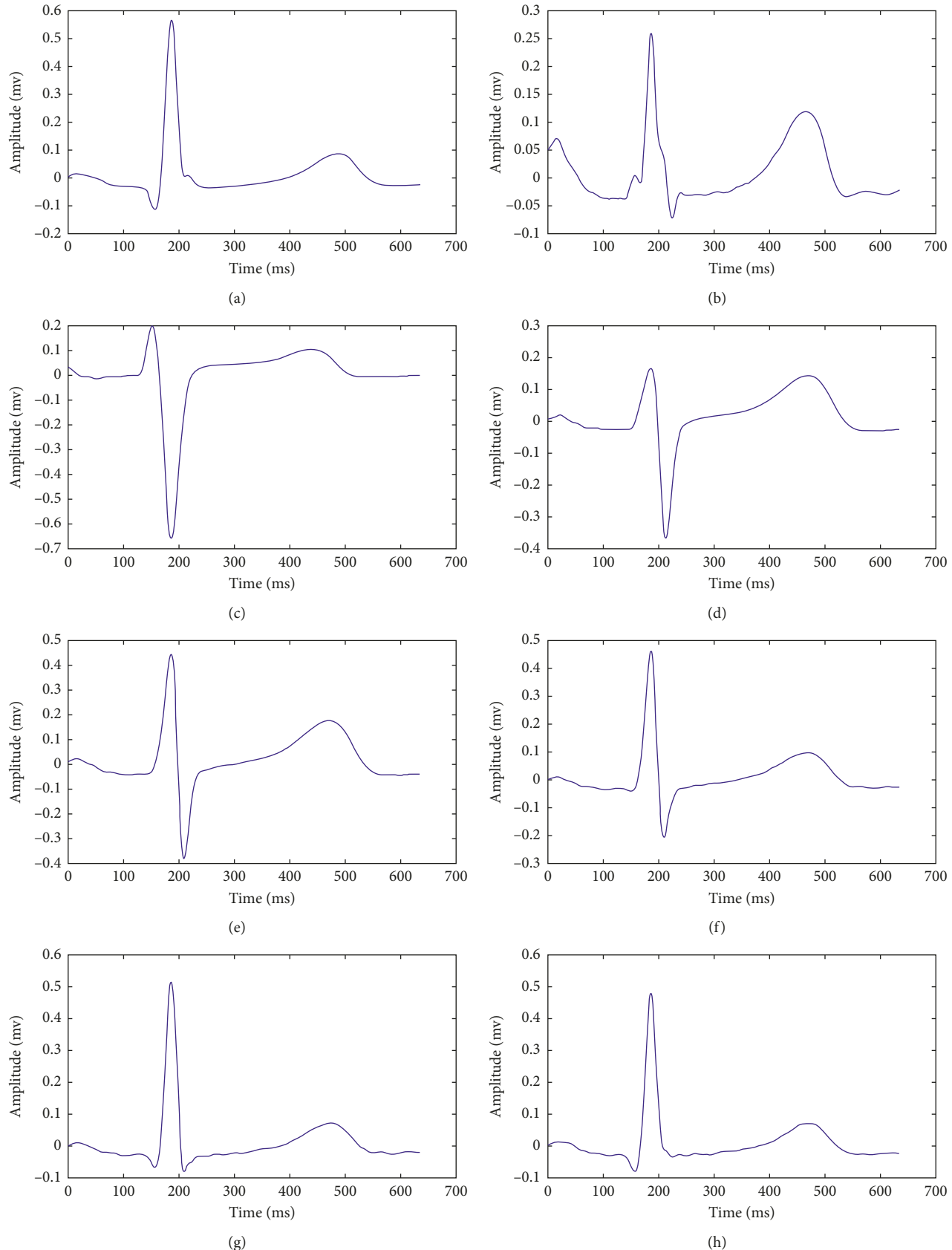


FIGURE 3: Templates for each of the 8 independent derivations of the ECG. (a) Deviation template I. (b) Deviation template II. (c) Deviation template V1. (d) Deviation template V2. (e) Deviation template V3. (f) Deviation template V4. (g) Deviation template V5. (h) Deviation template V6.

2.2.3. QRS Template Segmentation. The fiducial point of the QRS is determined using the SVM technique in each lead template (this point is denoted as Q_{ini}). The QRS detection algorithm provides the point QRS_1 corresponding to the QRS wave onset, the point QRS_2 corresponding to the R peak of the QRS, and the point QRS_{end} corresponding to the end of the QRS. A representative pair of values QRS_1 and QRS_2 for all leads is calculated using the procedure proposed by Starc and Schlegel [15] that enables calculation of the width of the QRS denoted as ΔQRS . The average Q_{ini} is obtained for the eight independent leads, and $Q_{\text{ini}0}$ is selected as the value for the lead that occurs earliest with respect to the average. The point QRS_{endo} is selected using a similar procedure but considering the average for QRS_{end} points in the eight leads. The points $Q_{\text{ini}0}$ and QRS_{endo} represent the initial and end points of the QRS wave. However, as suggested in [15], a larger interval is used by extending 20 ms before and 30 ms after the end, defining the points PQ_{break} and QT_{break} , as shown in Figure 4.

2.2.4. T-Wave Template Segmentation. The end of the T wave is estimated for each independent template lead using the SVM algorithm. This point is denoted as T_{end} . The point T_2 is located 30 ms after the T_{end} point, and T_1 is located 20 ms before the maximum of the absolute value of the T wave. Location for the T wave on each template is defined between points QT_{break} and T_2 , as shown in Figure 5.

2.2.5. Template QT Interval. The QT interval in each template lead is defined using the estimation for $Q_{\text{ini}0}$ and T_{end} . The calculation is performed as follows:

$$QT_{k,0} = T_{k,\text{end}} - Q_{k,\text{ini}0}, \quad (6)$$

where k is the lead considered.

2.3. Beat-to-Beat QT Interval Estimation. After considering the first twenty beats necessary for template calculation and QT interval initialization, our algorithm performs the beat-to-beat QT interval calculation. Each incoming beat is compared with respect to the lead template and accepted when the Pearson correlation coefficient is larger than a predefined threshold. The accepted beat is segmented by obtaining Q_{ini} and T_{end} using SVM techniques, and then, the points QRS_1 , QRS_2 , QRS_{end} , T_1 , T_2 , PQ_{break} , and QT_{break} are obtained using a procedure similar to the template segmentation. The calculation of the QT interval for the incoming beat is performed by shifting the incoming signal with respect to the template to obtain the maximal correlation within a particular beat region. The amount of shifting is used for updating the QT interval on each lead using the procedure proposed by Starc and Schlegel [15]. The beat-to-beat QT interval estimation is calculated as follows:

$$QT_{k,i} = QT_{k,0} + \Delta QRS_i + \Delta T_{k,i}, \quad (7)$$

where i is the incoming beat and k is the lead considered. The updating of the QT interval is the addition of the amount of shifting in the QRS template denoted as ΔQRS_i and the

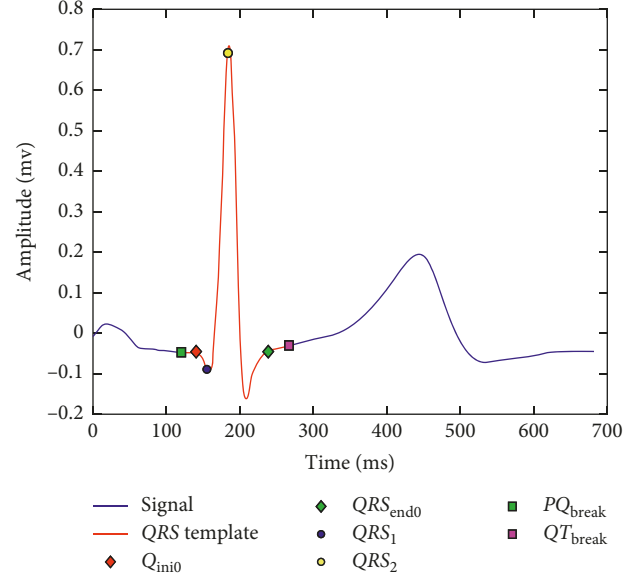


FIGURE 4: Template segmentation for obtaining PQ_{break} and QT_{break} .

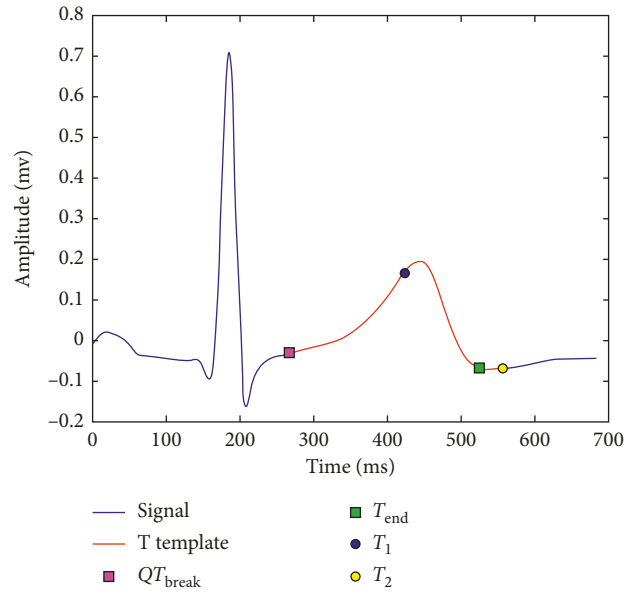


FIGURE 5: T-wave template segmentation between QT_{break} and T_2 .

T-wave template denoted as $\Delta T_{k,i}$. The amount of shifting is calculated as explained in Section 2.3.3. The system provides as a result the sequence of QT intervals for each of the leads, as well as their average.

2.3.1. Calculation of the Shifting for the QRS Template. The total amount of shifting for the QRS template is calculated considering two stages: in the first stage, the shifting of the segment $PQ_{\text{break}} - QT_{\text{break}}$ in the incoming beat with respect to the similar interval in the QRS template is calculated. This process is illustrated in Figure 6. During the second stage, the amount of shifting of the segment

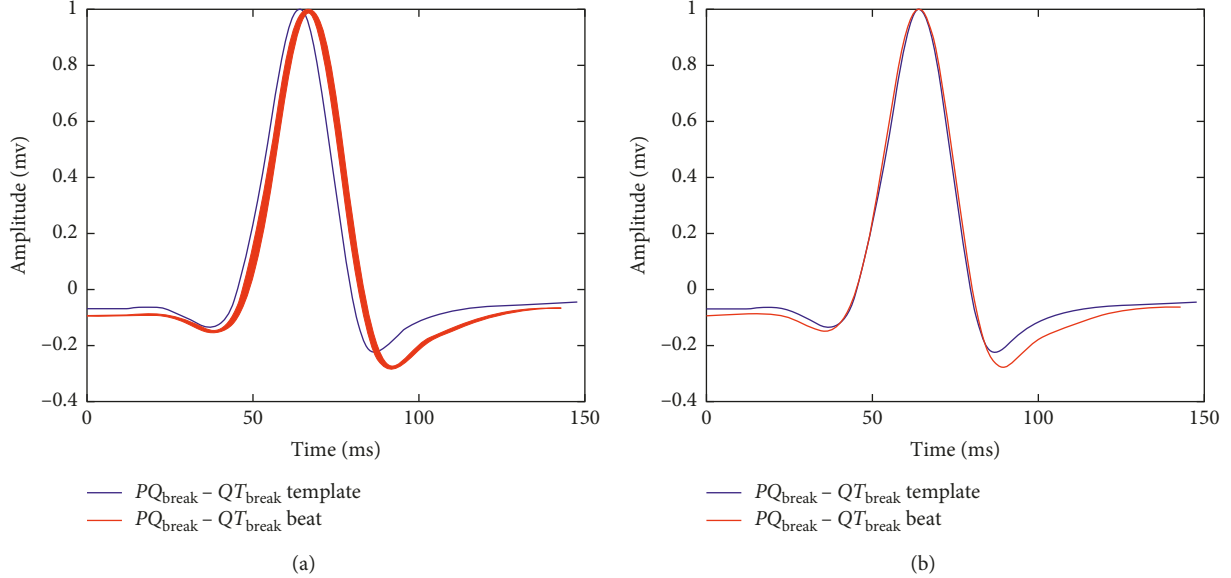


FIGURE 6: First stage for the alignment of the QRS template and the incoming beat. In (a), the initial alignment between the QRS template and the incoming beat is shown. In (b), both signals are aligned considering the procedure described in Section 2.3.3 for the interval between PQ_{break} and QT_{break} .

$\text{QRS}_1 - \text{QRS}_2$ in the incoming beat with respect to the similar segment in the QRS template is calculated. The alignment for this segment is shown in Figure 7. This procedure is performed for each lead for obtaining the array $\Delta\text{QRS}_{k,i}$, where k denotes the lead and i is the incoming beat. From this array, a representative ΔQRS_i is calculated as described for the QRS template segmentation.

2.3.2. Calculation of the Shifting for the T-Wave Template.

The total amount of shifting for the T -wave template is also performed using two stages: in the first stage, the shifting is calculated for the segment between QT_{break} and T_2 in the incoming beat with respect to the similar interval in the T -wave template. The alignment process is shown in Figure 8. During the second stage, the shifting is calculated for the T -wave considering the segment between T_1 and T_{end} in the segmented incoming beat with respect to the T -wave template. This alignment process is illustrated in Figure 9. This process is performed for each lead for obtaining the array of shifting for the T wave, $\Delta T_{k,i}$.

2.3.3. Temporal Shifting between Two Signals. The amount of shifting between a template denoted as $x(n)$ and the incoming signal denoted as $y(n)$ is calculated using the following functional:

$$J(\theta) = \min_{\theta} \sum_{n=1}^N (x(n) - y(n \pm \theta))^2, \quad (8)$$

where θ is the shifting in samples between signals and N is the length of the segment. The incoming signal is normalized with respect to the template.

2.3.4. Q_{ini} and T_{end} Calculation Using SVM. Two support vector machine algorithms were trained for detecting these points. The first SVM is trained for detecting the Q_{ini} point, and the second SVM was trained for detecting the T_{end} point. The training for the first SVM is performed using as feature ECG signal intervals that are centered at the actual Q_{ini} location (defined by an expert). These intervals are called *markers*, and other ECG signal intervals selected from other ECG regions are called *nonmarkers*. The second SVM is trained similarly for detecting the T_{end} point.

(1) *Training.* A total of 1800 beats are used for extracting features for training. 600 beats are extracted from hypertensive patients, 600 beats are extracted from chagasic patients, and 600 beats are extracted from control subjects. An additional set of 300 beats (100 from each patient group) is used for validation.

The annotation of the actual location of Q_{ini} and T_{end} was performed manually on each beat by a group of cardiologists.

(2) *Features Used for the SVM.* The SVM training is done based on selected reference points called *markers* and *nonmarkers*. For each of the selected points, the features used are a vector including signal samples located around the selected point as well as signal samples extracted from the discrete wavelet decomposition [31] of the beat selected.

The choice of the mother wavelet is based on research studies about the application of different wavelet families for QRS complex and *T*-wave detection [32, 33]. These research works recommend the utilization of the wavelet family Daubechies-4 (level 5) for QRS complex detection and Symlet-7 (level 6) for the *T* wave, because these wavelets show coefficients with greater amplitude and a pattern that roughly identifies the starting and the end point of the QRS

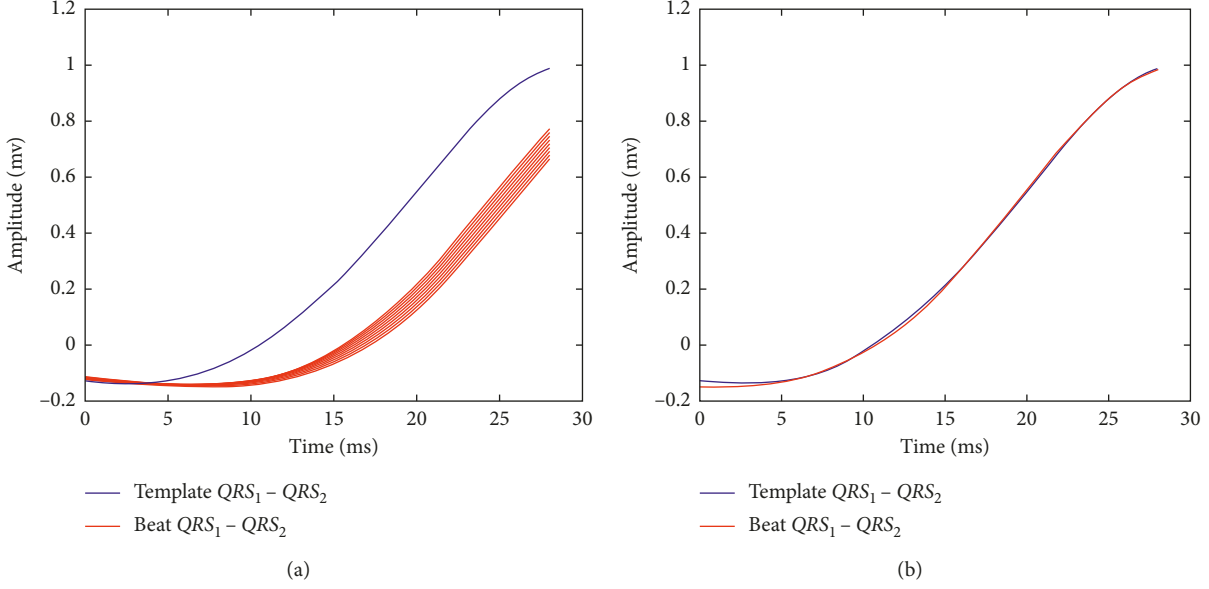


FIGURE 7: Second stage for the alignment of the QRS template and the incoming beat. In (a), the incoming beat is shifted with respect to the QRS template. In (b), both signals are aligned for the interval between QRS_1 and QRS_2 .

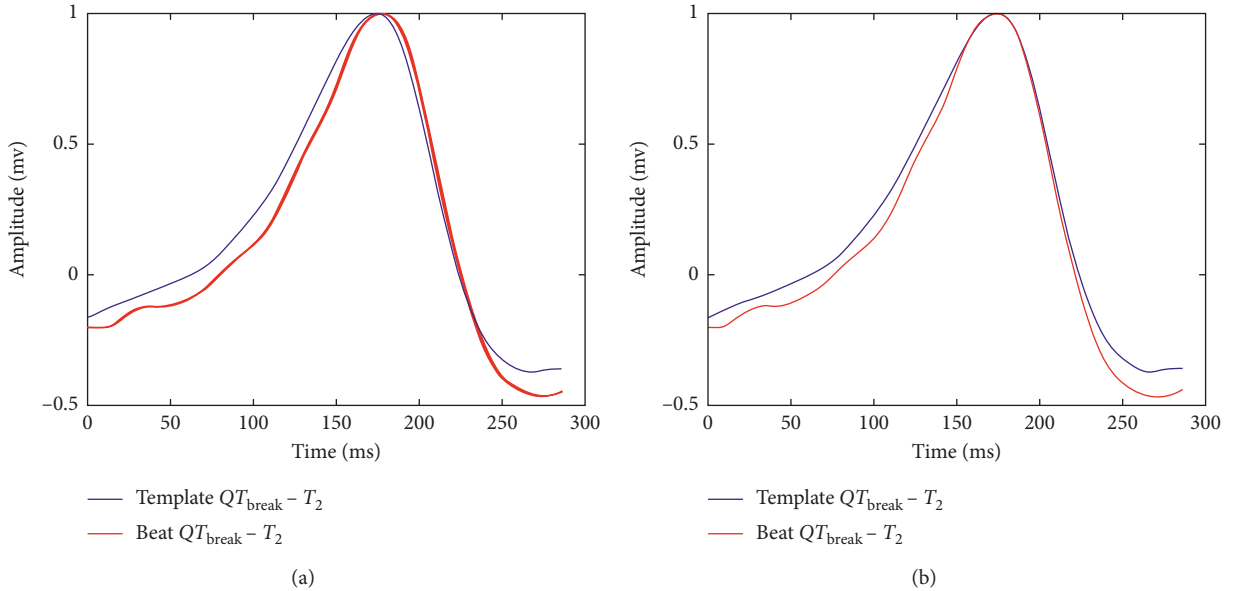


FIGURE 8: First stage for the alignment of the T-wave template and the incoming beat. In (a), the initial alignment between the T-wave template and the incoming beat is shown. In (b), both signals are aligned considering the procedure described in Section 2.3.3 for the interval between QT_{break} and T_2 .

complex, as well as the start and end point of the T wave. In consequence, this type of wavelets is used in the present work.

In this case, a level 5 reconstruction of the Daubechies-4 wavelet is used for the Q_{ini} detection. A level 6 reconstruction using the Symlet-7 is used for the T_{end} detection. The level of detail d6 offers relevant information about the T wave, by characterizing this pattern with two peaks: one positive and one negative including a zero crossing (Figure 10). Both reconstructed signals are obtained

with the same size as the QRS template. In Figure 11, the time matching between the original QRS signal and its wavelet reconstruction is shown. In this case, the level 5 detail of the Daubechies-4 wavelet decomposition is reconstructed using the inverse discrete wavelet transform (IDWT), where the zero crossings and peaks correlate with the Q , R , and S fiducial points.

(3) Features Vector. Each feature vector for *markers* and *nonmarkers* points is a vector including 41 samples, where

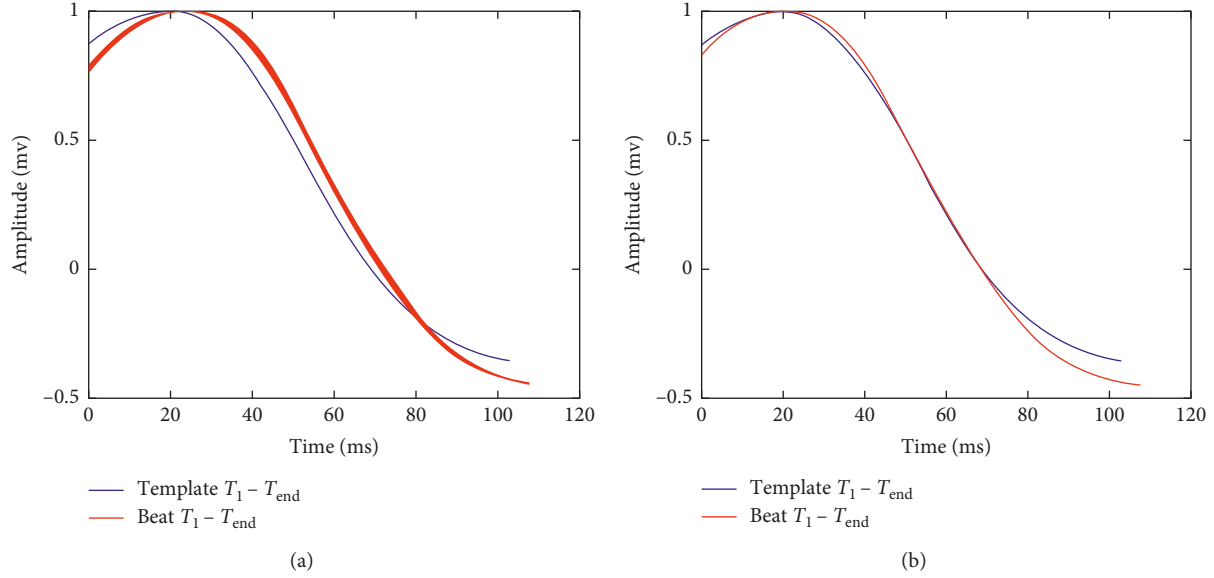


FIGURE 9: Second stage for the alignment of the T -wave template and the T wave in the incoming beat. In (a), the incoming T wave is shifted with respect to the T -wave template. In (b), both signals are aligned for the interval between T_1 and T_{end} .

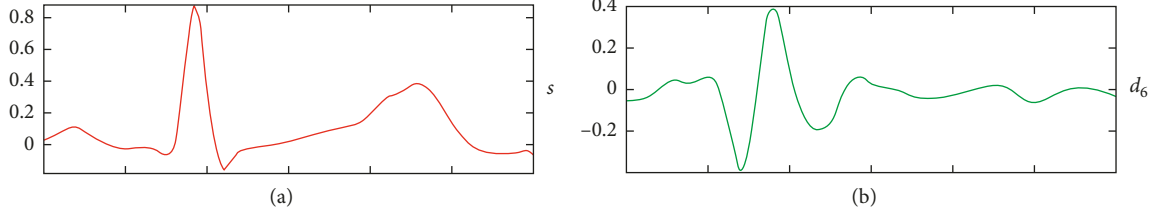


FIGURE 10: (a) A QRS signal template. (b) The IDWT reconstructed detail level 6 using Symlet-7. Two peaks are shown at the end of the T wave: one positive and one negative including a zero crossing.

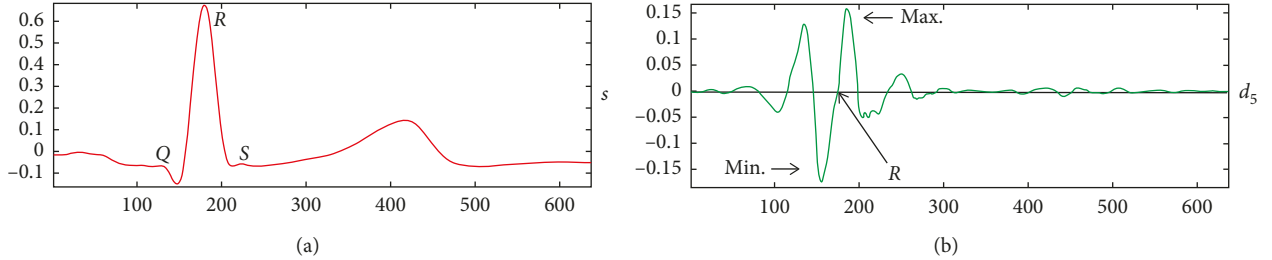


FIGURE 11: (a) A QRS signal template. (b) The reconstructed Daubechies-4 detail level 5. The zero crossings and peaks correlate with the Q , R , and S fiducial points.

samples 1 to 10 are the samples of the reconstructed wavelet detail located at the left of the selected Q_{ini} fiducial point. Samples 11 to 30 are the samples in the ECG beat located on a window centered on the selected point, and samples 31 to 41 are the samples of the reconstructed wavelet detail located at right of the selected Q_{ini} fiducial point. The construction of each marker vector is illustrated in Figure 12. At the left of the figure, the features vector content is shown. At the right, the window of the data source used for constructing the features vector is shown. The top and bottom are the reconstructed wavelet details of the beat, and at the center is

the data from the corresponding QRS beat. The markers for the T_{end} are constructed similarly; however, the wavelet decomposition uses a Symlet-7 wavelet, and the reconstructed detail 6 is considered for representing the marker. The length of the marker in this case is longer (51 samples) but the difference is that samples from 11 to 40 are extracted from the incoming beat. The rest of samples comes from the reconstructed wavelet detail.

(4) *Nonmarker Selection*. The *nonmarker* features vector is constructed with the same size and composition as the

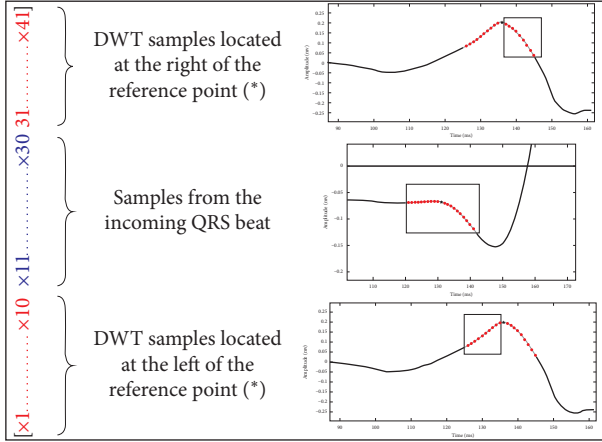


FIGURE 12: Feature vector for training the SVM used for detecting the Q_{ini} .

marker feature vector. However, in this case, the samples from the ECG beat and reconstructed wavelet detail are located outside from the marker regions. The location is selected at random from the beat and far from the fiducial point (Q_{ini} or T_{end}). For each *marker* vector, a number of five *nonmarker* vectors are selected. This procedure was performed for each of the 1800 beats considered for training.

(5) *Parameters Tuning.* Parameters gamma and sigma of the SVM were set using the following procedure: the detection of the fiducial point was performed in incoming beats extracted from the test set for classification accuracy estimation. The parameters were varied for obtaining a classification accuracy larger than 95%. The selected parameters for the Q_{ini} were gamma = 900 and sigma = 25 and for the T_{end} were gamma = 10 and sigma = 60.

(6) *Detection of Q_{ini} and T_{end} Using the Trained SVM.* The detection of Q_{ini} and T_{end} points is performed using the following procedure:

- (1) In each incoming beat, the level 5 reconstruction using the IDWT is obtained using the db4 wavelet. Similarly, the level 6 reconstruction using the Symlet-7 wavelet is calculated.
- (2) A search window is established, taking as reference the fiducial points calculated for the template on each lead: $Q_{k,\text{ini}0}$ and $T_{k,\text{end}}$. Thus, the search window for Q_{ini} is centered in the approximated initial fiducial point for the current lead, and it has a length of seven samples in the interval $[Q_{k,\text{ini}0} - 3, Q_{k,\text{ini}0}, Q_{k,\text{ini}0} + 3]$. Similarly, for the end of the T wave, the search window is located in the following interval: $[T_{k,\text{end}} - 3, T_{k,\text{end}}, T_{k,\text{end}} + 3]$.
- (3) For each of the points in the search window, the features vector is constructed and classified using the SVM. The points classified as *markers* are labeled with -1 and *nonmarker* with $+1$.
- (4) The points with a predicted label of -1 are selected. If there is more than one point with a predicted label

-1 , the first point of the group is selected as $Q_{k,\text{ini}}$. In the event that no point is labeled with -1 during the Q_{ini} detection, the parameter is set as $Q_{k,\text{ini}} = Q_{k,\text{ini}0}$ using the value calculated for the initial template. Concerning the T wave, when there is more than one point with predicted label -1 , the last point of the group is selected as $T_{k,\text{end}}$. Similarly, in the event of no points labeled with -1 , the parameter is set as $T_{k,\text{end}} = T_{k,\text{end}0}$ using the value calculated for the initial template.

Figure 13 shows a set of beats with different morphologies and its corresponding Q_{ini} and T_{end} points detected with the SVM.

3. Results and Validation of the Algorithm

3.1. *Validation Using Synthetic Signals.* A test using simulated signals was performed based on the work reported in [34]. A heartbeat was selected, and the amplitude of the T wave was varied by reducing their amplitude to 80%, 50%, and 30%. This QRS was replicated to obtain four signals with 300 beats, and white noise was added with zero mean and standard deviation of 3% of the original T -wave amplitude. Each signal was replicated to complete the eight independent leads. The set of signals have a constant QT of 391 msec; in consequence, the expected QT variability is 0 msec. The estimated QT for this experiment attained a standard deviation of 1.4 msec.

3.2. *Validation Using the Physionet Database.* The multilead QT estimation method is validated using a subset of the PTB Diagnostic ECG annotated database [25, 35]. This subset includes a group of 97 subjects where 80 belong to the control group, 7 are patients with hypertrophy, 6 are patients with valvular disease, and 4 are patients with myocarditis. The database contains the standard 12-lead ECG and the simultaneously recorded 3 Frank lead ECG. The signals are sampled at 1000 Hz, with a resolution of $0.5 \mu\text{V}$, and they have variable duration.

The validation process was performed by comparing the values of the QT interval calculated by our algorithm with respect to the manually estimated values of the QT parameter obtained by a group of Physionet experts (this information is provided in a text file for this dataset). The comparison is expressed in terms of the percent error; the percentage error obtained for each patient is reported as well as the mean and standard deviation of each of these measurements. Results of the validation using the Physionet PTB diagnostic ECG dataset are shown in the first row of Table 1. The first column corresponds to the group analyzed, the second column corresponds to the value (mean \pm std (min, max)) of the QT parameter in the Physionet reference file (QT phy.), the third column represents the value of QT calculated with our QT interval estimation algorithm (QT est.), and the last column shows the percentage error for QT interval (error (%)).

The annotated QT interval considering the 97 patients of the Physionet database is 387.83 ± 32.57 msec with a

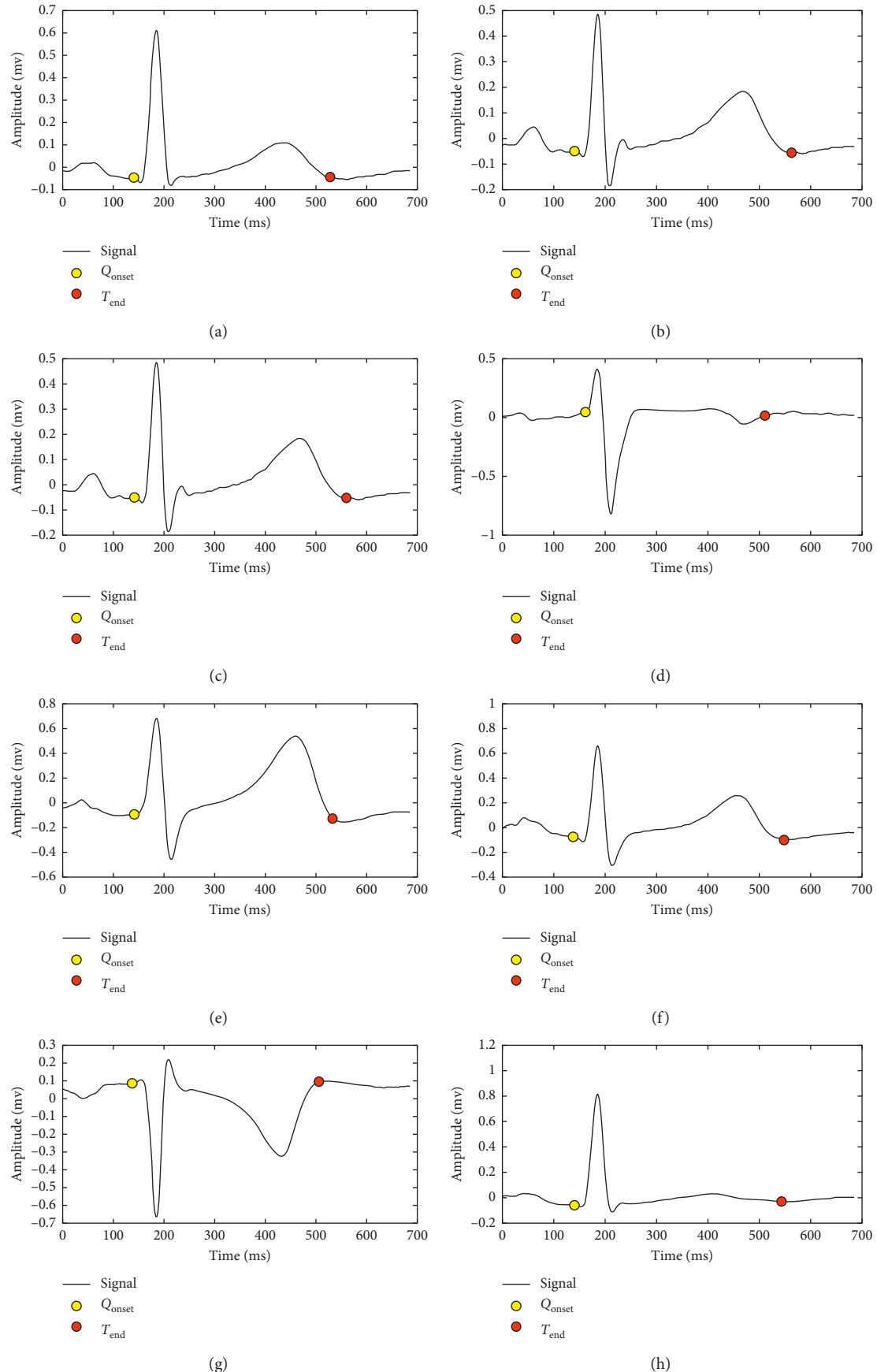


FIGURE 13: Detection of Q_{onset} and T_{end} points for different morphologies of the heartbeat.

TABLE 1: Validation of *QT* estimation using the Physionet database. The parameter is represented as mean \pm std. (min., max.).

Group	<i>QT</i> phy. (msec)	<i>QT</i> est. (msec)	Error (%)
Physionet dataset	387.83 ± 32.57 (317, 477)	384.74 ± 32.61 (316.9, 474.6)	2.60 ± 2.25 (0, 14.11)
Control subjects	386.96 ± 32.66 (317, 477)	384.64 ± 32.36 (316.9, 474.6)	2.35 ± 1.85 (0, 9.22)
Myocardial hypertrophy	380.14 ± 39.36 (317, 426)	375.64 ± 43.98 (321.3, 438.1)	4.36 ± 2.17 (1.42, 8.2)
Valvular heart disease	394.58 ± 30.79 (346, 426)	383.86 ± 32.67 (344.3, 438.1)	3.64 ± 5.20 (0.49, 14.11)
Myocarditis	408.37 ± 18.79 (385.5, 427.0)	403.85 ± 10.17 (395.1, 418.5)	3.11 ± 2.48 (0.27, 5.92)

minimum of 317.00 msec and a maximum of 477 msec. The estimated *QT* interval is 384.74 ± 32.61 msec, with a minimum of 316.90 msec and a maximum of 474.60 msec. The average percentage error is less than 5%, 2.60 ± 2.25 . The results obtained with this subset of the Physionet database are close to results reported by participants of the 2006 *QT* estimation challenge as Christov and Simova [19]. However, our approach is multilead and intended for *QT* variability analysis.

The second row of Table 1 reports the values corresponding to the *QT* interval obtained when processing the 80 electrocardiography records of control subjects using our algorithm compared with respect to the values provided in the Physionet reference file. The calculation of the interval *QT* indicates a good correlation with respect to the estimation provided in the Physionet dataset, presenting an average error of 2.35%. This set of control subjects belongs to the test set, and the percent of error is low demonstrating the good performance of the algorithm proposed. The third row of Table 1 reports the results obtained for the *QT* interval estimation, considering the 7 electrocardiography records of patients with myocardial hypertrophy. The results are compared with respect to the values provided in the Physionet reference file. In this case, the percentage of error for the mean *QT* interval is less than 5%, presenting a maximum error of 8.2% and a minimum error of 1.42%.

Results of *QT* intervals obtained when processing the 6 electrocardiographic records of patients with valvular heart disease using our algorithm with respect to the values provided in the Physionet reference file are presented in the fourth row of Table 1. The automatic estimation obtained by the algorithm provides good results, with an average error for the parameter *QT* less than 4%.

The fifth row of Table 1 reports the estimated *QT* interval values obtained when processing the 4 electrocardiography records of patients with myocarditis with respect to the values contained in the Physionet reference file. The values for the average percent error are 3.11%, and the standard deviation is 2.48%.

The results shown in Table 1 are satisfactory since this validation group (test data) is not part of the SVM training dataset and even though the average percent error for the mean and standard deviation is lower than 5%. These results show the good performance of the algorithm proposed in this work. Similarly, it is worth to mention there is a good correlation with respect to the values obtained for the *QT* interval reported in [36] and using the same Physionet dataset [26]. Results in Table 1 show globally an underestimation with respect to manual annotations of the Physionet dataset of 3.09 msec. Such underestimation could

be explained by the fact that annotators performed the manual estimation of the *QT* interval using only the lead II for the Physionet dataset [35] used in this validation. In contrast, our algorithm performs the *QT* estimation using a multilead approach, where all leads have a similar weight as we are simply averaging the *QT* intervals measured in each of the leads. A bias in the estimation using this dataset has also been reported by other researchers [37, 38] during the validation of multilead *QT* estimation algorithms.

3.3. Validation with a Dataset Acquired Using DIGICARDIAC. Results of the validation using 60 patients acquired with the DIGICARDIAC system are shown in Table 2. The validation for this dataset is performed by comparing the average *QT* interval in the eight leads with respect to the *QT* interval calculated using the Cardiosoft software [17]. The average *QT* interval estimated by the Cardiosoft software is 389.53 ± 30.37 msec with a minimum of 320.00 msec and a maximum of 450.00 msec. The average *QT* interval estimated using our algorithm is 391.62 ± 30.94 msec with a minimum of 318.40 msec and a maximum of 453.30 msec. The mean and standard deviations of the *QT* differences between our method and the Cardiosoft estimation are 2.49 ± 1.99 msec. The minimum is 0.08 msec, and the maximum is 8.23 msec.

Table 3 shows the numerical results corresponding to the parameter *QT* (msec) and *QTc* (msec), obtained by processing 20 electrocardiography records of hypertensive patients using our algorithm and the CardioSoft application. The average percentage error for *QT* is 1.74%, with a minimum value of 0.07% and a maximum value of 4.38%. Regarding the *QTc*, the average error of 2.66% is obtained with a minimum of 0.07% and a maximum of 5.20%. In this case, the error is below 6%, which is an acceptable measure.

The numerical results corresponding to the *QT* interval (msec) and *QTc* (msec) obtained by processing 20 electrocardiographic records of chagasic patients using the algorithm proposed and the CardioSoft application are shown in Table 4. The results provided by the proposed algorithm show a good accuracy as the average error for the parameters *QT* and *QTc* is less than 4%.

Table 5 shows the numerical results corresponding to the *QT* and *QTc* parameter in msec. In this case, the estimation is performed for 20 electrocardiography records of control subjects (healthy) using the proposed algorithm and compared with respect to the CardioSoft application. Concerning the *QT* interval, the mean value of the error was 2.54%, which is an acceptable measure. Regarding the *QTc*, the average error is 1.87%. These low error values show that the algorithm proposed could be useful for clinical application research.

TABLE 2: Validation considering 60 patients acquired with DIGICARDIAC. The validation is performed by comparing with respect to the Cardiosoft estimation.

	QT Cardiosoft (msec)	QT est. (msec)	Error (%)
Mean	389.53	391.62	2.49
Std. dev.	30.37	30.94	1.99
Min.	320.00	318.40	0.08
Max.	450.00	453.30	8.23

TABLE 3: QT interval (msec) and corrected QT (msec) for hypertensive patients with respect to the Cardiosoft application.

Parameter	QT est.	QT card.	QT E _r (%)	QTc est.	QTc card.	QTc E _r (%)
Mean	389.92	391.2	1.74	421.31	423.95	2.66
Std. dev.	26.63	29.63	1.36	21.58	20.49	1.33
Min.	348.8	348	0.07	379.7	380	0.07
Max.	447.6	450	4.38	452	464	5.20

TABLE 4: QT interval (msec) and corrected QTc (msec) for chagasic patients compared with respect to the Cardiosoft application.

Parameter	QT est.	QT card.	QT E _r (%)	QTc est.	QTc card.	QTc E _r (%)
Mean	400.05	395.1	3.20	423.29	414.8	3.38
Std. dev.	36.30	45.34	36.30	21.30	24.85	2.68
Min.	318.4	300	0.17	378.4	376	0.09
Max.	453.3	494	8.23	476.6	466	9.34

TABLE 5: QT interval (msec) and corrected QTc (msec) for healthy subjects with respect to the Cardiosoft application.

Parameter	QT est.	QT card.	QT E _r (%)	QTc est.	QTc card.	QTc E _r (%)
Mean	384.88	376.6	2.54	434.74	428.45	1.87
Std. dev.	28.64	27.95	2.06	25.97	21.76	1.76
Min.	332	320	0.20	392.8	387	0.04
Max.	434.2	420	6.5	492.4	466	6.05

The results shown in Tables 2–5 reflect the good performance of the methodology proposed in this research. The algorithm offers a good accuracy for the estimation of the QT and QTc intervals with respect to the estimated values obtained using the commercial software provided by CardioSoft. The comparison shows an average error of less than 4%.

4. Statistical Comparison between Patients and Control Subjects

In this section, we report the results of using one-way analysis of variance to determine statistically significant changes in the QT and QTc parameters between groups of patients. One-way analysis of variance was used to determine statistically significant changes ($p < 0.05$ and $F > 1$) between groups of patients. The use of this type of statistical analysis is justified because there are independent samples of two groups, and we want to contrast the null hypothesis (equality of means) with the hypothesis that the means are not equal.

Table 6 summarizes the results obtained for the QT and QTc parameter between hypertensive patients and control subjects in mean \pm SD.

TABLE 6: Comparison for the QT and QTc interval for hypertensive patients and control subjects.

Parameter	Hypertensive (mean \pm std. dev.)	Healthy (mean \pm std. dev.)	$p < 0.05$
QT (msec)	389.29 ± 27.06	383.56 ± 31.18	0
QTc (msec)	422.51 ± 25.31	434.56 ± 29.11	0

As can be seen, the average QTc and QT intervals are larger for the group of hypertensive patients in comparison with the control group. It is also important to note that there are statistically significant differences between hypertensive patients and control subjects represented by a value of $p < 0.05$. In general, the QT and QTc interval is prolonged in hypertensive patients with respect to healthy subjects as reported in [39–41].

Results obtained for the comparison of chagasic patients and healthy subjects concerning the QT and QTc interval are reported in Table 7. Results show statistically significant differences for QT and QTc intervals between control subjects and chagasic patients ($p < 0.05$). Concerning this disease, further research is still necessary considering a larger

TABLE 7: Comparison for the *QT* and *QTc* interval variability for chagasic patients with respect to control subjects.

Parameter	Chagasic (median \pm SD)	Healthy (median \pm SD)	<i>p</i> < 0.05
<i>QT</i> (msec)	398.90 \pm 35.0	383.56 \pm 31.18	0
<i>QTc</i> (msec)	420.60 \pm 27.01	434.56 \pm 29.11	0

group of patients and handling exclusion criteria concerning other diseases affecting the left ventricular repolarization [42].

5. Conclusions

The DIGICARDIAC system incorporates a software tool that enables accurate estimation of the multilead *QT* interval variability. The *QT* interval estimation algorithm uses high-performance machine learning techniques such as support vector machines for accurate estimation of fiducial points Q_{ini} and T_{end} on a multilead *QT* estimation framework. The algorithm was validated using the Physionet *QT* interval dataset, and additionally, a second validation was performed with respect to other commercially available software tools such as CardioSoft. Results obtained during the validation process are promising as the mean percentage error and deviation standard are low. The validation performed on hypertensive patients compared with respect to healthy subjects confirms the presence of *QT* interval prolongation in HTA patients with respect to the normal subjects. In contrast, the validation considering Chagas disease patients suggests the need of improving the clinical protocol considering a more strict selection of patients.

Data Availability

This research used a third-party dataset available online for validation purposes. The dataset is the PTB Diagnostic ECG Database available at <https://physionet.org/physiobank/database/ptbdb/>.

Conflicts of Interest

The authors declare that they have no conflicts of interest.

Acknowledgments

This work was supported by the Prometeo Project of the Ministry of Higher Education, Science, Technology and Innovation of the Republic of Ecuador. The work was also funded by the Research Coordination (CDCHT) from Universidad de los Andes in Venezuela and the Research Department from University of Cuenca (DIUC) in Ecuador.

References

- [1] G. A. Roth, C. Johnson, A. Abajobir et al., "Global, regional, and national burden of cardiovascular diseases for 10 causes, 1990 to 2015," *Journal of the American College of Cardiology*, vol. 70, no. 1, pp. 1–25, 2017.
- [2] B. Williams, G. Mancia, W. Spiering et al., "Ten commandments of the 2018 ESC/ESH guidelines for the management of arterial hypertension," *European Heart Journal*, vol. 39, no. 33, pp. 3021–3104, 2018.
- [3] F. A. Ehlert, D. S. Cannom, E. G. Renfroe et al., "Comparison of dilated cardiomyopathy and coronary artery disease in patients with life-threatening ventricular arrhythmias: differences in presentation and outcome in the avid registry," *American Heart Journal*, vol. 142, no. 5, pp. 816–822, 2001.
- [4] E. Braunwald, "Cardiomyopathies," *Circulation research*, vol. 121, no. 7, pp. 711–721, 2017.
- [5] C. Bern, "Chagas' disease," *New England Journal of Medicine*, vol. 373, no. 5, pp. 456–466, 2015.
- [6] D. F. Dávila, J. H. Donis, A. Torres, and J. A. Ferrer, "A modified and unifying neurogenic hypothesis can explain the natural history of chronic Chagas heart disease," *International Journal of Cardiology*, vol. 96, no. 2, pp. 191–195, 2004.
- [7] P. C. Pereira and E. Navarro, "Challenges and perspectives of chagas disease: a review," *Journal of Venomous Animals and Toxins including Tropical Diseases*, vol. 19, no. 1, p. 34, 2013.
- [8] J. F. Silva, L. S. A. Capettini, J. F. P. da Silva et al., "Mechanisms of vascular dysfunction in acute phase of *Trypanosoma cruzi* infection in mice," *Vascular Pharmacology*, vol. 82, pp. 73–81, 2016.
- [9] J. Perez and I. Molina, "Chagas disease," *The Lancet*, vol. 391, no. 10115, pp. 82–94, 2018.
- [10] S. Mangini, M. d. L. Higuchi, J. T. Kawakami et al., "Infectious agents and inflammation in donated hearts and dilated cardiomyopathies related to cardiovascular diseases, Chagas' heart disease, primary and secondary dilated cardiomyopathies," *International Journal of Cardiology*, vol. 178, pp. 55–62, 2015.
- [11] M. Baumert, A. Porta, M. A. Vos et al., "QT interval variability in body surface ECG: measurement, physiological basis, and clinical value: position statement and consensus guidance endorsed by the European heart rhythm association jointly with the esc working group on cardiac cellular electrophysiology," *Europace*, vol. 18, no. 6, pp. 925–944, 2016.
- [12] P. Postema and A. Wilde, "The measurement of the QT interval," *Current Cardiology Reviews*, vol. 10, no. 3, pp. 287–294, 2014.
- [13] E. de la Rosa, P. Paglini-Oliva, L. B. Prato et al., "Early detection of chronic asymptomatic chagas infection," *Medical Science Monitor*, vol. 24, pp. 4567–4571, 2018.
- [14] J. Bronzino and D. Peterson, "Biomedical signals, imaging, and informatics, ser," in *The Biomedical Engineering Handbook*, CRC, Taylor and Francis, Boca Raton, FL, USA, 4th edition, 2014.
- [15] V. Starc and T. T. Schlegel, "Real-time multichannel system for beat-to-beat QT interval variability," *Journal of Electrocardiology*, vol. 39, no. 4, pp. 358–367, 2006.
- [16] T. Schlegel, W. Kulecz, A. Feiveson et al., "Accuracy of advanced versus strictly conventional 12-lead ECG for detection and screening of coronary artery disease, left ventricular hypertrophy and left ventricular systolic dysfunction," *BMC Cardiovascular Disorders*, vol. 10, no. 1, p. 28, 2010.
- [17] Cardiosoft, "High frequency QRS electrocardiograph," 2009, <http://www.cardiosoft.com>.
- [18] P. Karjalainen, M. Tarvainen, and T. Laitinen, "Principal component regression approach for QT variability estimation," in *Proceedings of 27th Annual International Conference IEEE-EMBS*, Shanghai, China, 2005.

- [19] I. Christov and I. Simova, "Fully automated method for QT interval measurement in ECG," *Computers in Cardiology*, vol. 33, pp. 321–324, 2006.
- [20] Q. Xue and S. Reddy, "Algorithms for computerized QT analysis," *Journal of Electrocardiology*, vol. 30, pp. 181–186, 1998.
- [21] K. P. Murphy, *Machine Learning: A Probabilistic Perspective*, MIT Press, Cambridge, MA, USA, 2012.
- [22] S. Huang, N. Cai, P. P. Pacheco, S. Narandes, Y. Wang, and W. Xu, "Applications of support vector machine (SVM) learning in cancer genomics," *Cancer Genomics-Proteomics*, vol. 15, no. 1, pp. 41–51, 2018.
- [23] J. A. K. Suykens, J. De Brabanter, L. Lukas, and J. Vandewalle, "Weighted least squares support vector machines: robustness and sparse approximation," *Neurocomputing*, vol. 48, no. 1–4, pp. 85–105, 2002.
- [24] S. Berkaya, A. Uysal, E. Gunal, S. Ergin, S. Gunal, and M. Gulmezoglu, "A survey on ECG analysis," *Biomedical Signal Processing and Control*, vol. 43, pp. 216–235, 2018.
- [25] M. Oeff, H. Koch, R. Bousseljot, and D. Kreiseler, *The PTB diagnostic ECG database*, National Metrology Institute of Germany, Braunschweig, Germany, 2012, <http://www.physionet.org/physiobank/database/ptbdb>.
- [26] A. L. Goldberger, L. A. N. Amaral, L. Glass et al., "PhysioBank, PhysioToolkit, and PhysioNet," *Circulation*, vol. 101, no. 23, pp. e215–e220, 2000.
- [27] P. Laguna, R. G. Mark, A. Goldberg, and G. B. Moody, "A database for evaluation of algorithms for measurement of QT and other waveform intervals in the ECG," in *Computers in Cardiology 1997*, pp. 673–676, IEEE, Piscataway, NJ, USA, 1997.
- [28] N. Dugarte, R. Medina, L. Huiracocha, and R. Rojas, "Open source cardiology electronic health record development for DIGICARDIAC implementation," in *Proceedings of 11th International Symposium on Medical Information Processing and Analysis (SIPAIM 2015)*, p. 96810Y, International Society for Optics and Photonics, Cuenca, Ecuador, November 2015.
- [29] A. Savitzky and M. J. E. Golay, "Smoothing and differentiation of data by simplified least squares procedures," *Analytical chemistry*, vol. 36, no. 8, pp. 1627–1639, 1964.
- [30] M. Mneimneh, R. Povinelli, and M. Johnson, "Integrative technique for the determination of QT interval," in *Computers in Cardiology*, pp. 329–332, IEEE, Piscataway, NJ, USA, 2006.
- [31] R. Haddadi, E. Abdelmounim, M. El Hanine, and A. Belaguid, "Discrete wavelet transform based algorithm for recognition of QRS complexes," *World of Computer Science & Information Technology Journal*, vol. 4, no. 9, 2014.
- [32] L. Sörnmo and P. Laguna, *Bioelectrical Signal Processing in Cardiac and Neurological Applications*, Elsevier, Amsterdam, Netherlands, 2005.
- [33] P. Addison, *The Illustrated Wavelet Transform Handbook*, CRC Press, Boca Raton, FL, USA, 2017.
- [34] M. Baumert, V. Starc, and A. Porta, "Conventional QT variability measurement vs. template matching techniques: comparison of performance using simulated and real ECG," *PLoS One*, vol. 7, no. 7, Article ID e41920, 2012.
- [35] G. B. Moody, H. Koch, and U. Steinhoff, "The physionet/computers in cardiology challenge 2006: QT interval measurement," in *Computers in Cardiology*, pp. 313–316, IEEE, Piscataway, NJ, USA, 2006.
- [36] M. Mneimneh, R. Povinelli, and M. Johnson, "Integrate technique for the determination of QT interval," in *Proceedings of Computer in Cardiology Challenge*, vol. 33, pp. 329–332, Valencia, España, 2006.
- [37] R. Gregg, S. Babaeizadeh, D. Feild, E. Helfenbein, J. Lindauer, and S. Zhou, "Comparison of two automated methods for QT interval measurement," in *Computers in Cardiology*, pp. 427–430, IEEE, Piscataway, NJ, USA, 2007.
- [38] P. Langley, F. Smith, S. King, D. Zheng, A. Haigh, and A. Murray, "Fully automated computer measurement of QT interval from the 12-lead electrocardiogram," in *Computers in Cardiology*, pp. 345–348, IEEE, Piscataway, NJ, USA, 2006.
- [39] A. A. Akintunde, O. E. Ayodele, O. G. Opadijo, A. T. Oyedeleji, and O. B. Familoni, "QT interval prolongation and dispersion: epidemiology and clinical correlates in subjects with newly diagnosed systemic hypertension in Nigeria," *Journal of Cardiovascular Disease Research*, vol. 3, no. 4, pp. 290–295, 2012.
- [40] C. Passino, F. Franzoni, A. Gabutti, R. Poletti, F. Galetta, and M. Emdin, "Abnormal ventricular repolarization in hypertensive patients: role of sympatho-vagal imbalance and left ventricular hypertrophy," *International Journal of Cardiology*, vol. 97, no. 1, pp. 57–62, 2004.
- [41] J. Klimas, T. Stankovicova, J. Kyselovic, and L. Bacharova, "Prolonged QT interval is associated with blood pressure rather than left ventricular mass in spontaneously hypertensive rats," *Clinical and Experimental Hypertension*, vol. 30, no. 7, pp. 475–485, 2008.
- [42] T. T. Schlegel, R. Medina, D. Jugo et al., "Cardiac repolarization abnormalities and potential evidence for loss of cardiac sodium currents on electrocardiograms of patients with chagas heart disease," *Journal of Electrocardiology*, vol. 40, no. 6, pp. S132–S133, 2007.

